ACS Partner Journal
PRECISION CHEMISTRY

pubs.acs.org/PrecisionChem
Article

Controlled Synthesis and Phase Transition Mechanisms of Palladium Selenide: A First-Principles Study

Mingxiang Zhang, Aixinye Zhang, Hao Ren, Wenyue Guo, Feng Ding, and Wen Zhao*

Cite This: *Precis. Chem.* 2024, 2, 545−552

ABSTRACT: Using density functional theory, we carefully calculated the relative stability of monolayer, few-layer, and cluster structures with Penta $PdSe_2$, T-phase $PdSe_2$, and Pd_2Se_3-phase. We found that the stability of Penta $PdSe_2$ increases with the number of layers. The Penta $PdSe_2$, T-phase $PdSe_2$, and Pd_2Se_3 monolayers are all semiconducting, with band gaps of 1.77, 0.81, and 0.65 eV, respectively. The formation energy of palladium selenide clusters with different phase structures is calculated, considering the cluster size, stoichiometry, and chemical environment. Under typical experimental conditions, Pd_2Se_3 phase clusters are found to be dominant, having the lowest formation energy among all of the phases considered, with this dominance increasing as cluster size grows. Adjusting the Pd−Se ratio in the environment allows for controlled synthesis of specific palladium selenide phases, providing theoretical insights into the nucleation mechanisms of $PdSe_2$ and other transition metal chalcogenides.

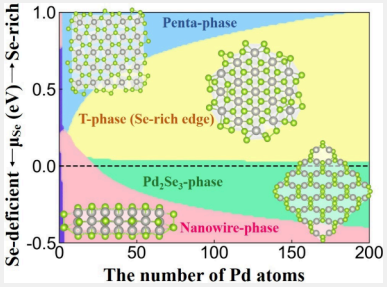

KEYWORDS: *palladium selenide, structural stability, electronic properties, cluster, formation energy*

1. INDUCTION

The recent research on two-dimensional layered transition metal dichalcogenides (TMDs) has revealed some interesting physics phenomena, including the quantum spin Hall effect,[1,2] valley polarization,[3,4] strong light−matter interactions,[5] and two-dimensional superconductivity,[6] indicating the potential application value of these materials in functional devices.[7−14] Many of these physical properties are influenced by their polymorphs, such as the semiconductor 2H phase, metallic 1T phase, topologically insulating 1T' phase, and Weyl semimetal Td phase;[15−18] therefore, precise control of the phases of TMDs is crucial for their application in functional devices.

Recently, some research on TMDs has gradually shifted to the tenth group of noble metal chalcogenides because they are predicted to have high carrier mobility[19] and good stability.[20−22] Among them, $PdSe_2$ is the most representative group-10 compound, as it has a unique orthorhombic crystal structure with a puckered pentagonal structure.[8,9,22] $PdSe_2$ also has other polymorphs, such as the T-phase $PdSe_2$, and metastable phases, including all possible phases found in this group.[23−25] Reports indicate that the wrinkled pentagonal structure of layered $PdSe_2$ can be effectively controlled through lithiation/delithiation processes, inducing a phase transition to the octahedral coordinated hexagonal T-phase $PdSe_2$.[26] Observations have shown that the T-phase $PdSe_2$ has significant light-capturing capabilities, indicating its potential candidacy for photovoltaic applications.[23,26]

Although $PdSe_2$ has other polymorphs and is expected to be applied in multiple fields, controlling the phase transition of $PdSe_2$ during the preparation process still poses a challenge. So far, in addition to the commonly used mechanical exfoliation method for preparing $PdSe_2$,[27] bottom-up methods for preparing high-quality MoS_2 and WSe_2, have also been employed to fabricate few-layer $PdSe_2$, such as molecular beam epitaxy,[14] predeposition of Pd layer sulfides,[28] and chemical vapor deposition (CVD).[29] In order to obtain even fewer layers of $PdSe_2$, some studies have suggested using oxygen plasma-assisted layer-by-layer thinning to prepare palladium diselenide.[30] Although these methods can produce large-area, high-quality few-layer $PdSe_2$, only the wrinkled pentagonal structure of $PdSe_2$ has been observed in the experimental products, greatly limiting the application of other polymorphs of $PdSe_2$. Interestingly, the occurrence of different polycrystalline forms in $PdSe_2$ is found to be layer-dependent, which is different from most transition metal dichalcogenides (TMDs).[31,32] Although the theoretical stability of monolayer $PdSe_2$ has been proven,[33] direct experimental evidence for the existence of monolayer Penta-$PdSe_2$ structure has not yet been obtained. Experimental findings indicate that the optimal monolayer structure of this material arises from the fusion of two pentaphase monolayers accompanied by the emission of

Received: June 22, 2024
Revised: September 17, 2024
Accepted: September 18, 2024
Published: September 30, 2024

https://doi.org/10.1021/prechem.4c00049
Precis. Chem. 2024, 2, 545−552

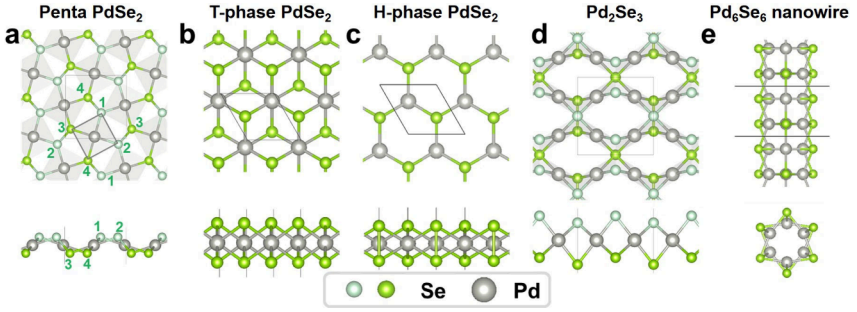

Figure 1. Top view (upper) and front view (lower) of optimized palladium selenide structures with different phases. (a) Penta $PdSe_2$. (b) T-phase $PdSe_2$. (c) H-phase $PdSe_2$. (d) Pd_2Se_3. (e) Pd_6Se_6 nanowire.

Se atoms. By combining scanning transmission electron microscopy (STEM) imaging and first-principles calculations, the authors determined that the resulting monolayer phase features a novel atomic structure with a chemical stoichiometry of Pd_2Se_3.[32] Therefore, even though few-layer $PdSe_2$ has been experimentally synthesized and investigated, little is known about its monolayer form on the experimental side.

In this article, we report a systematic study of palladium selenide clusters of different phases and sizes using first-principles calculations. First, we collected monolayer structures of different phases, including Penta $PdSe_2$, T-phase and H-phase $PdSe_2$, Pd_2Se_3, and Pd_6Se_6 nanowires. Two different DFT functionals were tested to calculate the structural characteristics and the dynamic stability of these phases. The formation energy and electronic properties of the monolayer structures of each phase were calculated. Then, cluster structures of different phases and sizes were built. The thermodynamic stability of the clusters was evaluated in different chemical environments, and the specific synthesis route of monolayer palladium selenide compounds was predicted. Further analysis revealed that the thermodynamic stability of clusters is influenced by the stoichiometry of the bulk and edges of the different phases. Our study provides theoretical guidance for the controllable synthesis of palladium selenide structures and advances the understanding of the transition metal dichalcogenide (TMD) family.

2. COMPUTATIONAL DETAILS

Density functional theory calculations (DFT) were performed using the Vienna Ab-initio Simulation Package (VASP),[34] with projector-augmented-wave (PAW) pseudopotentials[35] and a plane-wave expansion with a kinetic energy cutoff of 350 eV. In order to more accurately describe interlayer interactions and unify the energy scale, all clusters and few-layer structures were optimized using the strongly constrained and appropriately normed (SCAN) meta-generalized gradient approximation (meta-GGA).[36] Based on previously reported tests of the SCAN functional,[37] it has been found to predict formation energies more accurately than PBE for strongly bound compounds, including those containing chalcogens, which is precisely the category that $PdSe_2$ falls into. Moreover, previous studies have effectively employed the SCAN functional to investigate the $PdSe_2$ system, the calculated band structure overlaps with the measured ARPES spectra, demonstrating significant consistency.[38] Hence, all of the computational results presented in this study rely on the utilization of the SCAN functional. For a better description of the weak von der Waals (vdW) interactions, DFT-D3[39] correction was adopted. The Monkhorst−Pack scheme is used to sample the Brillouin zone with a 19 × 19 × 1 k-point mesh for monolayer and few-layer structures, 19 × 19 × 19 for bulk structures, and 1 × 1 × 1 for clusters. During the relaxation, the convergence criteria for energy and forces were set to 10^{-6} eV and 0.01 eV/Å, respectively. No spin-polarized calculation is considered in this work. The first-principles investigations of the phonon dispersion relations and phonon modes were performed by using the finite displacement method.[40]

The formation energies can be calculated using the following equation:

$$E_f(Pd_xSe_y) = E_{Pd_xSe_y} - x\mu_{Pd} - y\mu_{Se} \quad (1)$$

where μ_{Pd} and μ_{Se} are the chemical potential of Pd and Se, while x and y denote the quantity of Pd and Se atoms in the structure, respectively. A lower formation energy signifies greater stability.

3. RESULTS AND DISCUSSION

3.1. Structure and Stability

First, we attempt to elucidate the monolayer structure of palladium selenide and explore its stability. Figure 1 shows the optimized structures of the monolayer palladium selenide. The lattice constants are summarized in Table 1. We constructed

Table 1. Lattice Constants of Different Palladium Selenide Phases Calculated from Different DFT Functionals: (PBE-D3/SCAN-D3)

	a (Å)	*b* (Å)	c (Å)
T	3.657/3.699	3.657/3.699	
Penta	5.639/5.682	5.826/5.865	
H	3.928/3.938	3.928/3.938	
Pd_2Se_3	5.899/5.864	6.022/6.023	
nanowire			4.554/5.03

the 1T and 2H phases, which were found widely in other TMDs, and the unique puckered pentagonal structure of $PdSe_2$ (Penta-phase). Pd_2Se_3 monolayer is also considered, due to the previous report that monolayer Penta $PdSe_2$ is energetically unstable and tends to reconstruct into the Pd_2Se_3 phase.[32] To consider different stoichiometries, the nanowire structure Pd_6Se_6 is also introduced, which was first found in MoS_2, $MoSe_2$, and WSe_2.[41]

The stability of palladium selenide with different numbers of layers and different phases is evaluated from the perspective of formation energy. Figure 2 presents the formation energies per-atom, where the chemical potential of Pd (μ_{Pd}) uses the energy of pure Pd bulk, and μ_{Se} uses pure Se bulk. The

https://doi.org/10.1021/prechem.4c00049
Precis. Chem. 2024, 2, 545−552

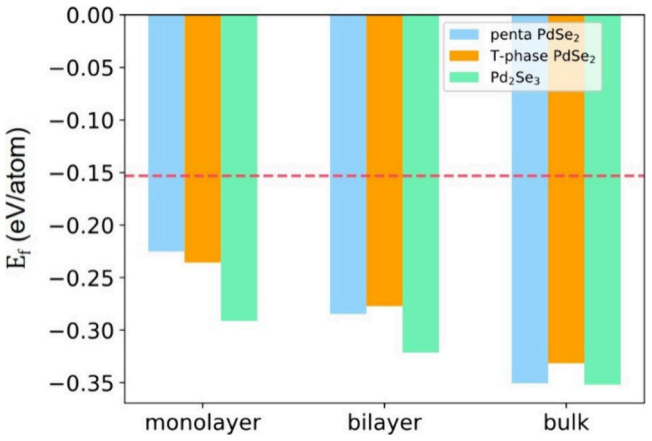

Figure 2. Formation energies of $PdSe_2$ with different phase structures and number of layers. The pink dashed line represents the formation energy of the Pd_6Se_6 nanowires. The formation energy of H-phase $PdSe_2$ is positive (+0.069 eV/atom), which is not shown in the figure.

formation energy of H-phase $PdSe_2$ is positive (+0.069 eV/atom), indicating thermodynamic instability, which is not shown in the figure. This aligns with the fact that H-phase $PdSe_2$ has never been synthesized experimentally. The pink dashed line in the figure represents the formation energy of Pd_6Se_6 nanowires, which is consistently higher than those of other palladium selenide phases, indicating poor thermodynamic stability. We can find that using the chemical potential we choose, Pd_2Se_3 always exhibits a better thermodynamic advantage regardless of the layer number. It implies that the number of layers has little impact on the stability of Pd_2Se_3.

For all of the Penta, T, and Pd_2Se_3 phases, increasing the number of layers will lower the formation energy, which comes from the contribution from interlayer vdW interactions. Especially, the relative stability of Penta and T-phase experiences a reversal, when the number of layers change from monolayer to bilayer and then to bulk. The formation energy of the Penta $PdSe_2$ monolayer is 0.01 eV/atom higher than the T-phase, while that of the Penta phase bulk is 0.02 eV/atom lower than the T-phase. It comes from the unique folded pentagonal structure of the Penta $PdSe_2$, leading to stronger interlayer vdW interactions of the Penta $PdSe_2$ (1.97 meV/Å^2 higher than the T-phase). From the perspective of atomic arrangement, as shown in Figure 1(a), the central Pd sublattice in the Penta $PdSe_2$ is formed by $PdSe_4$ units. Each Se_2 dimer (Se1−Se4 and Se2−Se3) crosses the boundary of the $PdSe_4$ unit and also diagonally traverses the main plane formed by Pd atoms. This arrangement prevents the in-plane $PdSe_2$ lattice from autonomously compensating for mechanical stress and requires interactions with the upper and lower layers of $PdSe_2$ to compensate for the mechanical stress caused by the Se_2 dimers.[42] Therefore, the per-atom formation energy of Penta $PdSe_2$ decreases as the number of layers increases, suggesting that a higher number of layers correlates with improved thermodynamic stability.

To test the dynamical stability of the five phases, we calculated the phonon spectra using the SCAN functional (see the red lines in Figure 3), and the results using the PBE functional are also shown (the black lines) as a comparison. It can be seen that both functionals yield no imaginary frequencies for the phonon spectra of T-phase $PdSe_2$ and Pd_2Se_3, indicating the dynamic stability of these three monolayer structures. However, in Figure 3a, if the atomic structure of Penta $PdSe_2$ is relaxed using the SCAN functional, there will be distinct imaginary frequencies in the phonon spectra, while the atomic structure relaxed using the PBE functional shows no imaginary frequencies in the phonon spectra. In Figure 3c and e, both H-phase $PdSe_2$ and Pd_6Se_6 nanowire structures show imaginary frequencies in the phonon spectra after relaxation using both the PBE and SCAN functionals, indicating the instability of these two structures. From the experimental results,[32] it is inferred that monolayer Penta $PdSe_2$ is energetically unstable and tends to reconstruct into the Pd_2Se_3 phase. Since the H-phase of $PdSe_2$ has the same stoichiometry as the Penta and T-phase, and there is the presence of imaginary frequencies in the phonon spectrum, it is not significant for subsequent research. Therefore, we excluded H-phase $PdSe_2$ in the subsequent calculations.

3.2. Electrical Properties

Experimental and theoretical studies have demonstrated that monolayer $PdSe_2$ exhibits high mobility and Seebeck coefficient,[8,43] which are beneficial for thermoelectric transport. We calculated the electronic properties of each phase. The band structure calculated along the high-symmetry path is shown in Figure 4, where high symmetry lines are generated from VASPKIT.[44] Here, the band gap is defined as the energy difference between the valence band (VB) and the conduction band (CB). The indirect band gaps of monolayer Penta $PdSe_2$, T-phase $PdSe_2$, and Pd_2Se_3, which exhibit semiconductor

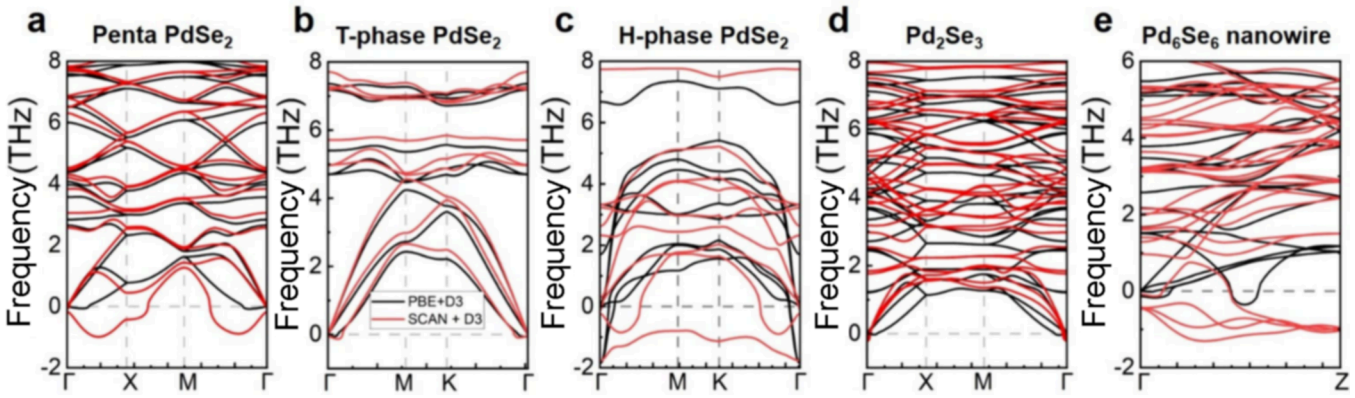

Figure 3. Phonon spectra of palladium sulfide with different phases calculated from different DFT functionals: PBE-D3 (black lines) and SCAN-D3 (red lines). (a) Penta $PdSe_2$. (b) T-phase $PdSe_2$. (c) H-phase $PdSe_2$. (d) Pd_2Se_3. (e) Pd_6Se_6 nanowire.

https://doi.org/10.1021/prechem.4c00049
Precis. Chem. 2024, 2, 545−552

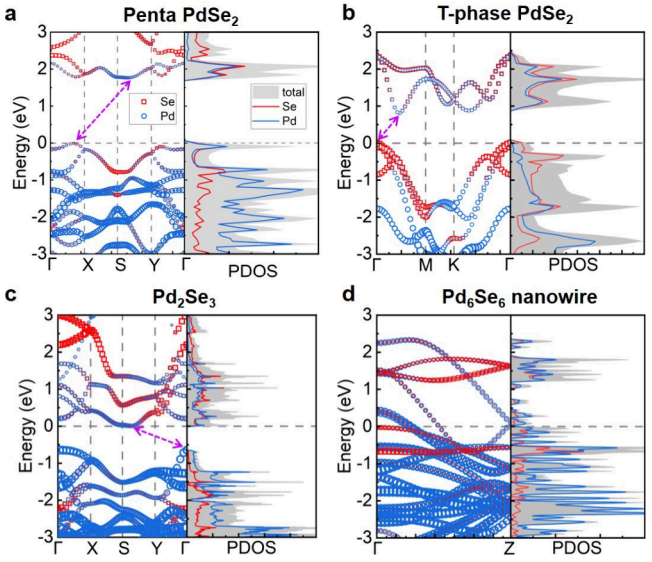

Figure 4. Band structure and projected density of states (PDOS) of different phases of the palladium sulfide monolayer. The Fermi level was set to zero and represented by a dotted line. The dashed arrows indicate the lowest energy transitions between the valence band maximum (VBM) and conduction band minimum (CBM). (a) Penta $PdSe_2$. (b) T-phase $PdSe_2$. (c) Pd_2Se_3. (d) Pd_6Se_6 nanowire.

characteristics, are 1.77, 0.81, and 0.65 eV, respectively. Our calculated band gap for monolayer Penta $PdSe_2$ is 1.77 eV, which lies between the values reported in previous studies using the optPBE functional[22] (1.37 eV) and the HSE06 method[45] (2.15 eV). For the Penta $PdSe_2$ monolayer, the VBM is located between the high-symmetry points Γ (0,0,0) and X (0.5,0,0), while the CBM is located between the high-symmetry points S (0.5,0.5,0) and Y (0,0.5,0). The predicted density of states suggests that the Pd element contributes relatively more to the VBM, while the Se element contributes relatively more to the CBM (Figure 4a). For T-phase $PdSe_2$, the VBM is located at the high-symmetry point Γ (0,0,0), and the CBM is located between the high-symmetry points Γ (0,0,0) and M (0,5,0,0). The predicted density of states suggests that the Se element contributes relatively more to both the VBM and the CBM (Figure 4b). For Pd_2Se_3, the VBM is located at the high-symmetry point Γ (0,0,0), and the CBM is located between the high-symmetry points S (0.5,0.5,0) and Γ (0,0,0). The predicted density of states suggests that the Pd element contributes relatively more to both the VBM and the CBM (Figure 4c). In Figure 4d, there is no band gap in the band structure of the Pd_6Se_6 nanowire, indicating its metallic nature along the axial direction.

3.3. Thermodynamic Stability and Phase Transition of Clusters

Then we explore the possible phase transition mechanism during the nucleation process of palladium selenide, driven by the energy reversion between the T phase and Penta phase in monolayer and few-layer forms and the interlayer fusion mechanism observed in experiments. We calculated the relative stability of palladium selenide clusters under different selenium chemical potentials, including Pd_2Se_3, Pd_6Se_6 nanowire, T-phase (Se-rich edge), T-phase (Se-deficient edge), and Penta-phase clusters. The Pd_6Se_6 nanowire phase is considered to achieve a diverse range of element stoichiometries.

The calculated formation energies are shown in Figure 5 (the dots), where the chemical potential of Se is selected as (a) −0.5, (b) 0.0, (c) 0.2, and (d) 0.6 eV relative to Se-bulk ($\mu_{Se\text{-}bulk}$ = 0 eV), which correspond to the representative Se chemical potentials of the four phases in Figure 6. And we choose the chemical potential of Pd in the monolayer T-phase

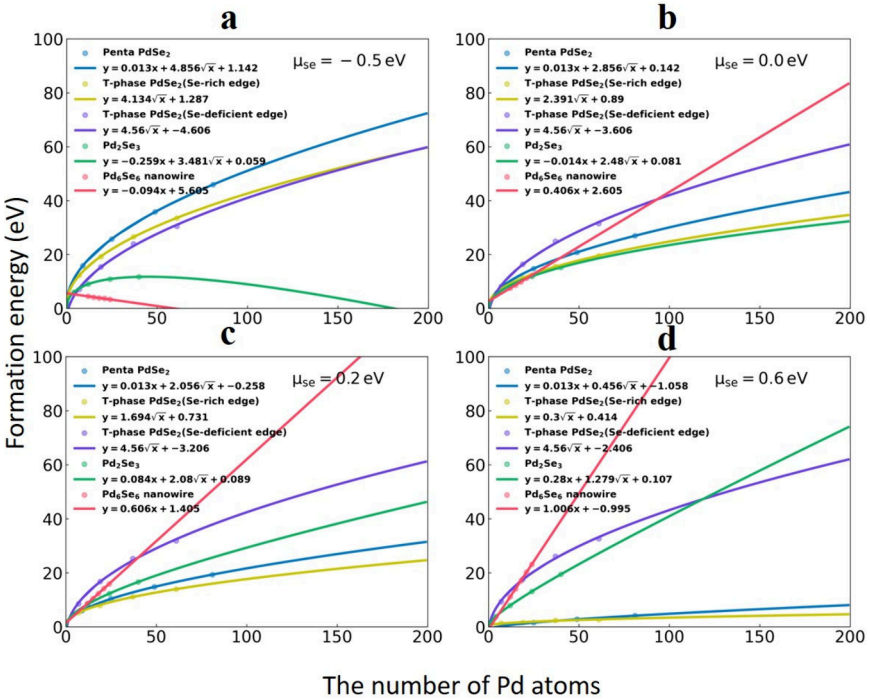

Figure 5. Relationship between the DFT-calculated formation energy of clusters (dots) and the number of Pd atoms (x) in the clusters. The lines represent the fitted curve. The chemical potential of Se is selected as (a) −0.5 eV, (b) 0.0 eV, (c) 0.2 eV, and (d) 0.6 eV relative to Se-bulk.

https://doi.org/10.1021/prechem.4c00049
Precis. Chem. 2024, 2, 545−552

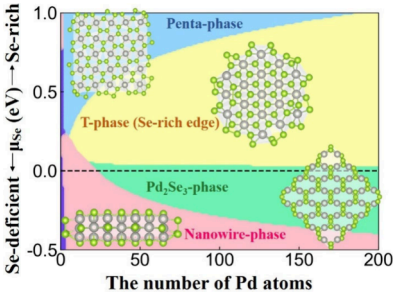

Figure 6. Diagram of the relative stabilities varied with the number of Pd atoms and the chemical potential of Se (μ_{Se}).

$PdSe_2$, because the formation energy of the T-phase is lowest in the monolayer $PdSe_2$ (see Figure 2):

$$\mu_{Pd} = \mu_{Pd-T} = (E_T - n_{Se}\mu_{Se})/n_{Pd} \quad (2)$$

We can see that the formation energy differences between the small clusters are relatively small. As the cluster size increases, the differences in the formation energy gradually become more pronounced. The formation energy of clusters with a 1D nanowire structure increases linearly with the number of Pd atoms, but this is not the case for other 2D clusters. Their formation energy is primarily influenced by the atoms at the edges and the differences in the arrangement of internal atoms compared with the most stable arrangement (T-phase).

The DFT-calculated formation energy as a function of size can be fitted accordingly. As a 1D structure, the formation energies of the nanowire phase can be fitted to a linear relationship:

$$\Delta E_f(Pd_xSe_y) = ax + c \quad (3)$$

where x is the number of Pd atoms, which is proportional to the length of the nanowire. The parameter c is the formation energy of the two end points of nanowire clusters. The formation energy of a 2D cluster can be fitted by

$$\Delta E_f(Pd_xSe_y) = ax + b\sqrt{x} + c \quad (4)$$

where x is proportional to the area of the cluster, and parameter b refers the intrinsic formation energy of the phase. For example, in the chemical environment of Figure 5a, a = 0.013 for Penta $PdSe_2$ and a = −0.259 for Pd_2Se_3 phase. In addition, since the chemical potential of Pd used is the chemical potential of Pd in the monolayer T-phase $PdSe_2$, b is equal to 0 for two types of T-phase clusters with different edge. This indicates that in this chemical potential, the formation energy of the Penta-phase monolayer is slightly higher than that of the T-phase monolayer, while the energy of the Pd_2Se_3 monolayer is lower than that of the T-phase monolayer. This suggests a Se-deficient chemical environment that favors the formation of clusters with a higher Pd−Se ratio. $\sqrt{x}$ is proportional to the edge length of the cluster, therefore the coefficient b is proportional to the edge formation energy of the cluster. The constant term c represents the formation energy of the cluster's vertices.

The values of the typical chemical potential, including DFT-calculated absolute energy and reference energy, which are required for subsequent use are listed in Table 2. The chemical potential of selenium (μ_{Se}) has two typical values. The first is the total energy of a Se atom in the Se bulk (μ_{Se_bulk} = −20.135 eV), which represents a Se-rich situation. The second is calculated using $\mu_{Se} = (\varepsilon_{PdSe_2} - \mu_{Pd\_bulk})/2$ = −20.661 eV,

Table 2. DFT-Calculated Energies of Various Systems, along with Corresponding Values from Different References (in eV)

	System	DFT-calculated energy	Set Se bulk as reference	Set Pd bulk as reference
	ε_{PdSe_2}	−74.305		
μ_{Se}	μ_{Se_bulk}	−20.135	0	
	$\mu_{isolated\_Se}$	−16.183	+3.592	
	$(\varepsilon_{PdSe_2}-\mu_{Pd\_bulk})/2$	−20.661	−0.526	
μ_{Pd}	μ_{Pd_bulk}	−32.984		0
	$\mu_{isolated\_Pd}$	− 28.427		+4.557
	$\varepsilon_{PdSe_2} - 2\ \mu_{Se\_bulk}$	−34.035		−1.051

which is half of the energy difference between Penta $PdSe_2$ bulk and the energy of Pd in its bulk form. It represents a Se-deficient situation. When the Se chemical potential equals the energy of an isolated Se atom ($\mu_{isolated\_Se}$ = −16.183 eV), it represents an extremely Se-rich situation, which is not achievable under typical experimental conditions. Thus, a Se chemical potential range of −20.661 to −20.135 eV corresponds to more common experimental conditions, which is −0.526 to 0 eV if μ_{Se_bulk} is used as the reference energy. However, considering the energy of an isolated Se atom, which is +3.592 eV relative to μ_{Se_bulk}, we have considered a broader range of chemical potentials (−0.5 to +1 eV) to cover all relevant scenarios for a more comprehensive and systematic analysis. Our findings indicate that both Penta $PdSe_2$ and T-phase (Se-rich edge) $PdSe_2$ appear in the region where the chemical potential of Se is greater than 0, as shown in Figure 6.

From Figure 5, it can be seen that the calculated formation energies align well with the fitted curves. In Figure 5b, When the cluster structure is smaller (with less than 20 Pd atoms in the cluster), the formation energy of the Pd_6Se_6 nanowire-type clusters is lower, indicating that it is easier for Pd_6Se_6 nanowire-type clusters to form during the nucleation process. When the number of Pd atoms in the cluster increases, the formation energy of the Pd_2Se_3-type clusters is lower instead, indicating that Pd_2Se_3-type clusters are easier to form (in general, μ_{Se} < 0 eV).

We collected the most stable phases for all Se chemical potentials in the range of $x \leq 200$ and obtained a phase diagram, as shown in Figure 6. When μ_{Se} is very small, indicating an extreme lack of Se in the environment, the stability of the Pd_6Se_6 nanowire nucleus has a greater advantage, in terms of energy. As the Se chemical potential increases, the Pd_2Se_3 phase gradually becomes dominant in the phase diagram, and the critical size also decreases. As the Se chemical potential continues to rise, the T-phase and the Penta phase appear successively in the phase diagram. This is consistent with experimental STEM observation.[32] Under electron beam irradiation, Se atoms tend to detach from the material and escape, which leads to a decrease of μ_{Se}, thereby promoting the formation of Pd_2Se_3.

In typical experimental conditions, the chemical potential of Se is generally below that of bulk Se, ranging from −0.526 to 0 eV relative to the energy of bulk Se. As shown in the green region of Figure 6, when μ_{Se} is between 0 and −0.526 eV relative to bulk Se, clusters with the Pd_2Se_3 phase and nanowire phase are dominant. Moreover, as the cluster size increases, the proportion of clusters with the Pd_2Se_3 phase

https://doi.org/10.1021/prechem.4c00049
Precis. Chem. 2024, 2, 545−552

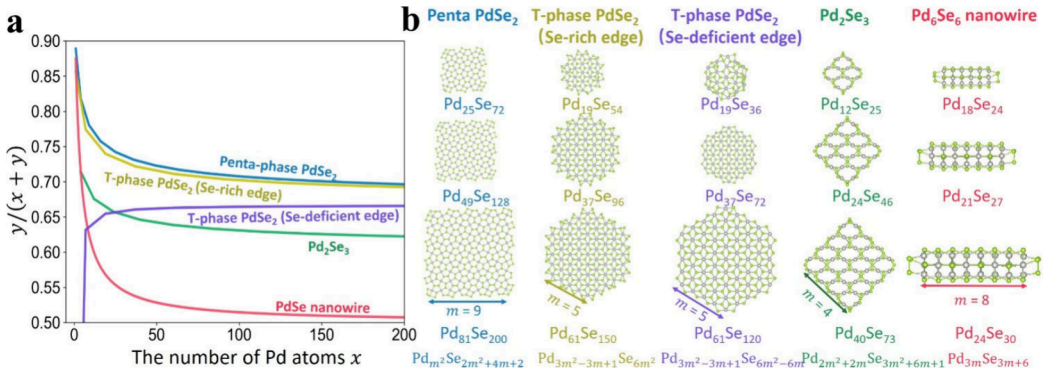

Figure 7. (a) Relative content of Se, $y/(x + y)$, changes with the size of the clusters in different phases, represented by the number of Pd atoms in the cluster, x. (b) Optimized structures with different phases and edges. The chemical formulas for each cluster and the general chemical formulas for each type of cluster are denoted accordingly. In these formulas, m represents the number of Pd atoms at the edge.

becomes more significant. Therefore, the experimentally observed monolayer palladium selenide is most likely in the Pd_2Se_3 phase.

The relative stability of clusters with different phase structures varies with the chemical potential of Se and the size of the clusters rather than solely depending on the inherent stability of the phases themselves. We hypothesize that this variability may arise from the differing ratios of Pd and Se atoms at the edges of clusters with different phases, which in turn affects their stability in varying chemical environments. Therefore, in Figure 7a, we plotted the curve showing the variation of Se content in the clusters as a function of cluster size, while Figure 7b presents the general chemical formulas of each phase cluster, derived from the changes in the Pd and Se atomic ratios with cluster size, along with the structures of these clusters.

The Se content in the clusters is illustrated in Figure 7a. The Se content in Pd_6Se_6 nanowire-type clusters is the lowest, and as the cluster size increases, the proportion of edge Se atoms in Pd_6Se_6 nanowire-type clusters decreases, causing the Se content to gradually approach 0.5. Therefore, in a Se-deficient environment (very low μ_{Se} in Figure 6), Pd_6Se_6 nanowire-type clusters are more likely to form despite the inherent instability of the nanowire phase. The Se content in Pd_2Se_3-type clusters is higher than in Pd_6Se_6 nanowire-type clusters and also higher than the stoichiometric ratio of 3/5 for the Pd_2Se_3 phase because excess Se is needed to saturate the edges. Hence, after the increase in the chemical potential of Se Pd_2Se_3-type clusters are more likely to form. Both the T phase and Penta phase have a stoichiometric ratio of 1:2, but the Se content in the corresponding clusters is higher than 0.66, with the Se content in the Penta phase being slightly higher than that in the T phase, especially for smaller cluster sizes. Thus, when the chemical potential of Se increases to 0 eV and continues to rise (which is not achievable under typical experimental conditions), the T phase and Penta phase successively dominate. The final phase structure of the material depends on the phase structure during nucleation, and the final product's phase structure can be controlled by regulating the phase structure of the clusters. Therefore, we can achieve the controlled synthesis of palladium selenide phase structures by regulating the ratio of Pd and Se in the environment.

4. CONCLUSIONS

In summary, the crystal structure of layered palladium selenide and nanowire $PdSe_2$ was demonstrated, and two different DFT functionals were tested. The electrical properties of other structures of $PdSe_2$, except for the H-phase, were then calculated, showing that layered palladium selenide is a semiconductor with an indirect bandgap. The formation energy calculation results for palladium selenide structures with different numbers of layers indicate that the monolayer Penta $PdSe_2$ is not energetically dominant. These findings suggest the existence of a phase transition during the growth process of $PdSe_2$. Finally, calculations and fittings of the formation energies for clusters of different sizes indicate that the chemical potential of Se in the environment, cluster size, and atomic structure all have an impact on their formation energies. By adjusting the ratio of Pd and Se in the environment, we can achieve the controlled synthesis of palladium selenide phase structures. This also provides theoretical guidance for understanding the nucleation mechanisms of other transition metal chalcogenides.

AUTHOR INFORMATION

Corresponding Author

Wen Zhao − *School of Materials Science and Engineering, China University of Petroleum (East China), Qingdao 266580 Shandong, China;* orcid.org/0000-0002-1118-8155; Email: zhaowen@upc.edu.cn

Authors

Mingxiang Zhang − *School of Materials Science and Engineering, China University of Petroleum (East China), Qingdao 266580 Shandong, China*

Aixinye Zhang − *School of Materials Science and Engineering, China University of Petroleum (East China), Qingdao 266580 Shandong, China*

Hao Ren − *School of Materials Science and Engineering, China University of Petroleum (East China), Qingdao 266580 Shandong, China;* orcid.org/0000-0001-9206-7760

Wenyue Guo − *School of Materials Science and Engineering, China University of Petroleum (East China), Qingdao 266580 Shandong, China;* orcid.org/0000-0002-7537-984X

Feng Ding − *Institute of Technology for Carbon Neutrality, Shenzhen Institute of Advanced Technology, Chinese Academy of Sciences, Shenzhen 518055, China; Faculty of Materials Science and Energy Engineering, Shenzhen University of Advanced Technology, Shenzhen 518055, China*

https://doi.org/10.1021/prechem.4c00049
Precis. Chem. 2024, 2, 545−552

Complete contact information is available at:
https://pubs.acs.org/10.1021/prechem.4c00049

Notes

The authors declare no competing financial interest.

■ ACKNOWLEDGMENTS

We acknowledge the financial support from the National Natural Science Foundation of China (12104513), the Shandong Provincial Natural Science Foundation of China (ZR2020QA050), and the Taishan Scholars Program of Shandong Province (tsqn201909071).

■ REFERENCES

(1) Zhang, Y.; Tan, Y.-W.; Stormer, H. L.; Kim, P. Experimental Observation of the Quantum Hall Effect and Berry's Phase in Graphene. *Nature* **2005**, *438* (7065), 201−204.
(2) Qian, X.; Liu, J.; Fu, L.; Li, J. Quantum Spin Hall Effect in Two-Dimensional Transition Metal Dichalcogenides. *Science* **2014**, *346* (6215), 1344−1347.
(3) Xiao, D.; Liu, G.-B.; Feng, W.; Xu, X.; Yao, W. Coupled Spin and Valley Physics in Monolayers of \mathrmMoS_2 and Other Group-VI Dichalcogenides. *Phys. Rev. Lett.* **2012**, *108* (19), 196802.
(4) Zeng, H.; Dai, J.; Yao, W.; Xiao, D.; Cui, X. Valley Polarization in MoS2Monolayers by Optical Pumping. *Nat. Nanotechnol.* **2012**, *7* (8), 490−493.
(5) Zhang, S.; Sun, D.; Sun, J.; Ma, K.; Wei, Z.; Park, J. Y.; Coffey, A. H.; Zhu, C.; Dou, L.; Huang, L. Unraveling the Effect of Stacking Configurations on Charge Transfer in WS2 and Organic Semiconductor Heterojunctions. *Precis. Chem.* **2023**, *1* (7), 443−451.
(6) Saito, Y.; Nojima, T.; Iwasa, Y. Highly Crystalline 2D Superconductors. *Nat. Rev. Mater.* **2017**, *2* (1), 16094.
(7) Novoselov, K. S.; Geim, A. K.; Morozov, S. V.; Jiang, D.; Zhang, Y.; Dubonos, S. V.; Grigorieva, I. V.; Firsov, A. A. Electric Field Effect in Atomically Thin Carbon Films. *Science* **2004**, *306* (5696), 666−669.
(8) Chow, W. L.; Yu, P.; Liu, F.; Hong, J.; Wang, X.; Zeng, Q.; Hsu, C.-H.; Zhu, C.; Zhou, J.; Wang, X.; Xia, J.; Yan, J.; Chen, Y.; Wu, D.; Yu, T.; Shen, Z.; Lin, H.; Jin, C.; Tay, B. K.; Liu, Z. High Mobility 2D Palladium Diselenide Field-Effect Transistors with Tunable Ambipolar Characteristics. *Adv. Mater.* **2017**, *29* (21), 1602969.
(9) Puretzky, A. A.; Oyedele, A. D.; Xiao, K.; Haglund, A. V.; Sumpter, B. G.; Mandrus, D.; Geohegan, D. B.; Liang, L. Anomalous Interlayer Vibrations in Strongly Coupled Layered PdSe2*. *2D Mater.* **2018**, *5* (3), 035016.
(10) Liang, Q.; Wang, Q.; Zhang, Q.; Wei, J.; Lim, S. X.; Zhu, R.; Hu, J.; Wei, W.; Lee, C.; Sow, C.; Zhang, W.; Wee, A. T. S. High-Performance, Room Temperature, Ultra-Broadband Photodetectors Based on Air-Stable PdSe2. *Adv. Mater.* **2019**, *31* (24), 1807609.
(11) Wang, Q. H.; Kalantar-Zadeh, K.; Kis, A.; Coleman, J. N.; Strano, M. S. Electronics and Optoelectronics of Two-Dimensional Transition Metal Dichalcogenides. *Nat. Nanotechnol.* **2012**, *7* (11), 699−712.
(12) Roy, K.; Padmanabhan, M.; Goswami, S.; Sai, T. P.; Ramalingam, G.; Raghavan, S.; Ghosh, A. Graphene-MoS2 Hybrid Structures for Multifunctional Photoresponsive Memory Devices. *Nat. Nanotechnol.* **2013**, *8* (11), 826−830.
(13) Lopez-Sanchez, O.; Lembke, D.; Kayci, M.; Radenovic, A.; Kis, A. Ultrasensitive Photodetectors Based on Monolayer MoS2. *Nat. Nanotechnol.* **2013**, *8* (7), 497−501.
(14) Li, E.; Wang, D.; Fan, P.; Zhang, R.; Zhang, Y.-Y.; Li, G.; Mao, J.; Wang, Y.; Lin, X.; Du, S.; Gao, H.-J. Construction of Bilayer PdSe2 on Epitaxial Graphene. *Nano Res.* **2018**, *11* (11), 5858−5865.
(15) Yang, H.; Kim, S. W.; Chhowalla, M.; Lee, Y. H. Structural and Quantum-State Phase Transitions in van Der Waals Layered Materials. *Nat. Phys.* **2017**, *13* (10), 931−937.
(16) Manzeli, S.; Ovchinnikov, D.; Pasquier, D.; Yazyev, O. V.; Kis, A. 2D Transition Metal Dichalcogenides. *Nat. Rev. Mater.* **2017**, *2* (8), 17033.
(17) Saraf, D.; Chakraborty, S.; Kshirsagar, A.; Ahuja, R. In Pursuit of Bifunctional Catalytic Activity in PdS2 Pseudo-Monolayer through Reaction Coordinate Mapping. *Nano Energy* **2018**, *49*, 283−289.
(18) Fang, Y.; Lv, X.; Lv, Z.; Wang, Y.; Zheng, G.; Huang, F. Electron-Extraction Engineering Induced 1T''-1T' Phase Transition of Re0.75V0.25Se2 for Ultrafast Sodium Ion Storage. *Adv. Sci.* **2022**, *9* (36), 2205680.
(19) Zhang, W.; Huang, Z.; Zhang, W.; Li, Y. Two-Dimensional Semiconductors with Possible High Room Temperature Mobility. *Nano Res.* **2014**, *7* (12), 1731−1737.
(20) Zhao, Y.; Qiao, J.; Yu, Z.; Yu, P.; Xu, K.; Lau, S. P.; Zhou, W.; Liu, Z.; Wang, X.; Ji, W.; Chai, Y. High-Electron-Mobility and Air-Stable 2D Layered PtSe2 FETs. *Adv. Mater.* **2017**, *29* (5), 1604230.
(21) Zhao, Y.; Qiao, J.; Yu, P.; Hu, Z.; Lin, Z.; Lau, S. P.; Liu, Z.; Ji, W.; Chai, Y. Extraordinarily Strong Interlayer Interaction in 2D Layered PtS2. *Adv. Mater.* **2016**, *28* (12), 2399−2407.
(22) Oyedele, A. D.; Yang, S.; Liang, L.; Puretzky, A. A.; Wang, K.; Zhang, J.; Yu, P.; Pudasaini, P. R.; Ghosh, A. W.; Liu, Z.; Rouleau, C. M.; Sumpter, B. G.; Chisholm, M. F.; Zhou, W.; Rack, P. D.; Geohegan, D. B.; Xiao, K. PdSe2: Pentagonal Two-Dimensional Layers with High Air Stability for Electronics. *J. Am. Chem. Soc.* **2017**, *139* (40), 14090−14097.
(23) Lei, W.; Zhang, S.; Heymann, G.; Tang, X.; Wen, J.; Zheng, X.; Hu, G.; Ming, X. A New 2D High-Pressure Phase of $PdSe_2$ with High-Mobility Transport Anisotropy for Photovoltaic Applications. *J. Mater. Chem. C* **2019**, *7* (7), 2096−2105.
(24) Gu, Y.; Zhang, L.; Cai, H.; Liang, L.; Liu, C.; Hoffman, A.; Yu, Y.; Houston, A.; Puretzky, A. A.; Duscher, G.; Rack, P. D.; Rouleau, C. M.; Meng, X.; Yoon, M.; Geohegan, D. B.; Xiao, K. Stabilized Synthesis of 2D Verbeekite: Monoclinic $PdSe_2$ Crystals with High Mobility and In-Plane Optical and Electrical Anisotropy. *ACS Nano* **2022**, *16* (9), 13900−13910.
(25) Kempt, R.; Kuc, A.; Heine, T. Two-Dimensional Noble-Metal Chalcogenides and Phosphochalcogenides. *Angew. Chem., Int. Ed.* **2020**, *59* (24), 9242−9254.
(26) Jakhar, M.; Singh, J.; Kumar, A.; Pandey, R. First-Principles Study of the Hexagonal T-Phase $PdSe_2$ Monolayer and Its Application in Solar Cells. *J. Phys. Chem. C* **2020**, *124* (49), 26565−26571.
(27) Velický, M.; Donnelly, G. E.; Hendren, W. R.; McFarland, S.; Scullion, D.; DeBenedetti, W. J. I.; Correa, G. C.; Han, Y.; Wain, A. J.; Hines, M. A.; Muller, D. A.; Novoselov, K. S.; Abruña, H. D.; Bowman, R. M.; Santos, E. J. G.; Huang, F. Mechanism of Gold-Assisted Exfoliation of Centimeter-Sized Transition-Metal Dichalcogenide Monolayers. *ACS Nano* **2018**, *12* (10), 10463−10472.
(28) Zeng, L.-H.; Wu, D.; Lin, S.-H.; Xie, C.; Yuan, H.-Y.; Lu, W.; Lau, S. P.; Chai, Y.; Luo, L.-B.; Li, Z.-J.; Tsang, Y. H. Controlled Synthesis of 2D Palladium Diselenide for Sensitive Photodetector Applications. *Adv. Funct. Mater.* **2019**, *29* (1), 1806878.
(29) Jia, L.; Wu, J.; Yang, T.; Jia, B.; Moss, D. J. Large Third-Order Optical Kerr Nonlinearity in Nanometer-Thick $PdSe_2$ 2D Dichalcogenide Films: Implications for Nonlinear Photonic Devices. *ACS Appl. Nano Mater.* **2020**, *3* (7), 6876−6883.
(30) Hoffman, A. N.; Gu, Y.; Tokash, J.; Woodward, J.; Xiao, K.; Rack, P. D. Layer-by-Layer Thinning of $PdSe_2$ Flakes via Plasma Induced Oxidation and Sublimation. *ACS Appl. Mater. Interfaces* **2020**, *12* (6), 7345−7350.
(31) Silva, A.; Polcar, T.; Kramer, D. Phase Behaviour of (Ti:Mo) S2 Binary Alloys Arising from Electron-Lattice Coupling. *Comput. Mater. Sci.* **2021**, *186*, 110044.
(32) Lin, J.; Zuluaga, S.; Yu, P.; Liu, Z.; Pantelides, S. T.; Suenaga, K. Novel Pd 2 Se 3 Two-Dimensional Phase Driven by Interlayer Fusion in Layered PdSe 2. *Phys. Rev. Lett.* **2017**, *119* (1), 016101.
(33) Qin, D.; Yan, P.; Ding, G.; Ge, X.; Song, H.; Gao, G. Monolayer PdSe2: A Promising Two-Dimensional Thermoelectric Material. *Sci. Rep.* **2018**, *8* (1), 2764.

(34) Kresse, G.; Furthmüller, J. Efficient Iterative Schemes for Ab Initio Total-Energy Calculations Using a Plane-Wave Basis Set. *Phys. Rev. B* **1996**, *54* (16), 11169−11186.
(35) Kresse, G.; Joubert, D. From Ultrasoft Pseudopotentials to the Projector Augmented-Wave Method. *Phys. Rev. B* **1999**, *59* (3), 1758−1775.
(36) Sun, J.; Ruzsinszky, A.; Perdew, J. P. Strongly Constrained and Appropriately Normed Semilocal Density Functional. *Phys. Rev. Lett.* **2015**, *115* (3), 036402.
(37) Isaacs, E. B.; Wolverton, C. Performance of the Strongly Constrained and Appropriately Normed Density Functional for Solid-State Materials. *Phys. Rev. Mater.* **2018**, *2* (6), 063801.
(38) Ryu, J. H.; Kim, J.-G.; Kim, B.; Kim, K.; Kim, S.; Park, J.-H.; Park, B.-G.; Kim, Y.; Ko, K.-T.; Lee, K. Direct Observation of Orbital Driven Strong Interlayer Coupling in Puckered Two-Dimensional PdSe2. *Small* **2022**, *18* (9), 2106053.
(39) Grimme, S.; Antony, J.; Ehrlich, S.; Krieg, H. A Consistent and Accurate Ab Initio Parametrization of Density Functional Dispersion Correction (DFT-D) for the 94 Elements H-Pu. *J. Chem. Phys.* **2010**, *132* (15), 154104.
(40) Ackland, G. J.; Warren, M. C.; Clark, S. J. Practical Methods in Ab Initio Lattice Dynamics. *J. Phys.: Condens. Matter* **1997**, *9* (37), 7861.
(41) Lin, J.; Cretu, O.; Zhou, W.; Suenaga, K.; Prasai, D.; Bolotin, K. I.; Cuong, N. T.; Otani, M.; Okada, S.; Lupini, A. R.; Idrobo, J.-C.; Caudel, D.; Burger, A.; Ghimire, N. J.; Yan, J.; Mandrus, D. G.; Pennycook, S. J.; Pantelides, S. T. Flexible Metallic Nanowires with Self-Adaptive Contacts to Semiconducting Transition-Metal Dichalcogenide Monolayers. *Nat. Nanotechnol.* **2014**, *9* (6), 436−442.
(42) Kuklin, A. V.; Ågren, H.; Avramov, P. V. Structural Stability of Single-Layer $PdSe_2$ with Pentagonal Puckered Morphology and Its Nanotubes. *Phys. Chem. Chem. Phys.* **2020**, *22* (16), 8289−8295.
(43) Sun, J.; Shi, H.; Siegrist, T.; Singh, D. J. Electronic, Transport, and Optical Properties of Bulk and Mono-Layer PdSe2. *Appl. Phys. Lett.* **2015**, *107* (15), 153902.
(44) Wang, V.; Xu, N.; Liu, J.-C.; Tang, G.; Geng, W.-T. VASPKIT: A User-Friendly Interface Facilitating High-Throughput Computing and Analysis Using VASP Code. *Comput. Phys. Commun.* **2021**, *267*, 108033.
(45) Kuklin, A. V.; Ågren, H. Quasiparticle Electronic Structure and Optical Spectra of Single-Layer and Bilayer \mathrmPdSe_2: Proximity and Defect-Induced Band Gap Renormalization. *Phys. Rev. B* **2019**, *99* (24), 245114.

https://doi.org/10.1021/prechem.4c00049
Precis. Chem. 2024, 2, 545−552